Dentomaxillofacial Radiology (2023) 52, 20220301

birpublications.org/dmfr

RESEARCH ARTICLE

Development and validation of apparent diffusion coefficient histogram-based nomogram for predicting malignant transformation of sinonasal inverted papilloma

[1]Meng Qi, [1]Zhipeng Xia, [1]Fang Zhang, [1]Yan Sha and [2]Jiliang Ren

[1]Department of Radiology, Eye & ENT Hospital of Fudan University, Shanghai, China; [2]Department of Radiology, Shanghai Ninth People's Hospital, Shanghai Jiao Tong University School of Medicine, Shanghai, China

Objectives: To develop and validate a nomogram based on whole-tumour histograms of apparent diffusion coefficient (ADC) maps for predicting malignant transformation (MT) in sinonasal inverted papilloma (IP).
Methods: This retrospective study included 209 sinonasal IPs with and without MT, which were assigned into a primary cohort (n = 140) and a validation cohort (n = 69). Eight ADC histogram features were extracted from the whole-tumour region of interest. Morphological MRI features and ADC histogram parameters were compared between the two groups (with and without MT). Stepwise logistic regression was used to identify independent predictors and to construct models. The predictive performances of variables and models were assessed using the area under the curve (AUC). The optimal model was presented as a nomogram, and its calibration was assessed.
Results: Four morphological features and seven ADC histogram parameters showed significant differences between the two groups in both cohorts (all $p < 0.05$). Maximum diameter, loss of convoluted cerebriform pattern, ADC_{10th} and $ADC_{Skewness}$ were identified as independent predictors to construct the nomogram. The nomogram showed significantly better performance than the morphological model in both the primary (AUC, 0.96 *vs* 0.88; $p = 0.006$) and validation (AUC, 0.96 *vs* 0.88; $p = 0.015$) cohorts. The nomogram showed good calibration in both cohorts. Decision curve analysis demonstrated that the nomogram is clinically useful.
Conclusions: The developed nomogram, which incorporates morphological MRI features and ADC histogram parameters, can be conveniently used to facilitate the pre-operative prediction of MT in IPs.
Dentomaxillofacial Radiology (2023) **52**, 20220301. doi: 10.1259/dmfr.20220301

Cite this article as: Qi M, Xia Z, Zhang F, Sha Y, Ren J. Development and validation of apparent diffusion coefficient histogram-based nomogram for predicting malignant transformation of sinonasal inverted papilloma. *Dentomaxillofac Radiol* (2023) 10.1259/dmfr.20220301.

Keywords: paranasal sinus; papilloma; apparent diffusion coefficient; histogram; inverted

Introduction

The sinonasal inverted papilloma (IP) is a benign tumour with a risk of malignant transformation (MT).[1] Sinonasal IPs with and without MT have different prognoses and treatments. When a patient's IP is suspected of MT, more extensive surgical resection is indicated, combined with postoperative adjuvant radiotherapy or chemoradiotherapy.[2,3] Therefore, accurate diagnosis of inverted papilloma with malignant transformation (MT-IP) is strongly associated with the choice of treatment strategy. However, it remains challenging to identify MT-IP in clinical practice; although endoscopic biopsy is the current standard procedure, it has the limitations of an invasive nature and sampling errors.[4]

Correspondence to: Jiliang Ren, E-mail: renjiliang2016@163.com; Yan Sha, E-mail: cjr.shayan@vip.163.com

Received 13 September 2022; revised 04 January 2023; accepted 23 January 2023; published online 17 February 2023
The authors Meng Qi and Zhipeng Xia contributed equally to the work.

MRI with diffusion-weighted imaging (DWI) has been widely used for the diagnosis and pre-operative evaluation of sinonasal tumours. The apparent diffusion coefficient (ADC) obtained from DWI, which represents an objective measure of tissue-specific diffusion capacity, has been used to differentiate benign and malignant sinonasal tumours quantitatively.[5–7] Some studies have suggested that the ADC, obtained from conventional measurements, could help to determine the biological behaviour of IP, with lower values observed in MT-IP.[6] However, conventional measurements mainly depend on the mean value of voxels within regions of interest (ROIs). Because intratumour heterogeneity is not accounted for in these methods, they do not represent the whole tumour and often miss slight but important tumour information.[8,9] To avoid this sampling error, a whole-tumour histogram analysis method that involves placing a ROI on the entire lesion has been proposed to evaluate tumour characteristics more precisely.[10]

Recently, a preliminary study reported that whole-tumour ADC histogram analysis may provide valuable information for predicting MT-IP.[11] However, in that small sample study, an independent validation analysis was not performed. Therefore, the aim of this study is to develop and validate a nomogram that incorporates both the ADC histogram parameters and morphological features for predicting sinonasal MT-IP, based on large samples (n = 209).

Methods and patients

Patients

This retrospective study was approved by our institutional ethics committee and the requirement to gather informed consent was waived. One experienced radiologist reviewed the medical records of Eye & ENT Hospital of Fudan University to identify patients treated from January 2015 to November 2021. We included patients who: (1) were histopathologically diagnosed with sinonasal IP or MT-IP, with complete pathological data, and (2) underwent MRI examinations, including DWI, before treatment. We excluded patients who had: (1) poor quality images, from artefacts or body motion, (2) tumours smaller than 10 mm along the short axis or (3) tumours that were recurrent lesions. In all, 209 patients were included in this study and assigned to a primary cohort (n = 140) or a validation cohort (n = 69) according to their imaging examination number. The primary cohort was used to train the predictive model, and the validation cohort was used to assess the performance and generalization of the model.

Magnetic resonance imaging technique

MRI was performed using a 3 T Siemens MRI system (Magnetom Verio or Prisma; Siemens Medical, Erlangen, Germany) with a 12-channel head coil. The MRI protocol included the following sequences: axial T_1 weighted imaging, axial and coronal fat-suppressed T_2 weighted imaging, axial DWI and axial and coronal fat-suppressed contrast-enhanced T_1 weighted imaging. Axial DWI was undertaken using a readout-segmented echoplanar imaging sequence. The imaging parameters for DWI were as follows: repetition time, 4700 ms; echo time, 66 ms; flip angle, 90°; field of view, 180× 180 mm; matrix, 160 × 160; slice thickness, 3 mm; interslice gap, 1.2 mm; b, 0 and 1000 s/mm^2. The gradient directions were x, y and z. The ADC map was calculated using a monoexponential fit.

Image analysis

Morphological MRI evaluation: Two radiologists who were blinded to histopathological outcomes and clinical information (with 6 and 8 years of experience in head and neck imaging) independently reviewed all images. If disagreements occurred, a senior radiologist (with 16 years of experience) would be called on to resolve the differences. Morphological features of each lesion were evaluated as follows: (1) three-dimensional maximum diameter; (2) bony erosion; (3) orbit or intracranial invasion; (4) loss of convoluted cerebriform pattern (CCP). We defined a CCP on a T_2 weighted or contrast-enhanced T_1 weighted image as a mixture of linear or curvilinear hyper- or hypointense striations, visualised in the solid portion of the tumour.[8]

Whole-tumour ADC histogram analysis: Whole-tumour segmentation was performed using ITK-SNAP (v. 3.6.0; www.itksnap.org). The ROIs were manually drawn slice by slice to cover the entire tumour to the greatest extent possible. Visible cystic or necrotic components and areas of haemorrhage were avoided by referring to T_2 weighted images and contrast-enhanced T_1 weighted images. Histogram analysis was performed using the Radiomics module of 3D Slicer (v. 4.11.0; www.slicer.org), which is based on the open-source Python package Pyradiomics (www.radiomics.io). Eight first-order statistical features, namely, mean (ADC_{Mean}), median (ADC_{Median}), 10th percentile (ADC_{10th}), 90th percentile (ADC_{90th}), skewness ($ADC_{Skewness}$), kurtosis ($ADC_{Kurtosis}$), uniformity ($ADC_{Uniformity}$) and entropy ($ADC_{Entropy}$), were extracted from whole-tumour ROIs. The number of histogram bins was set to 64.

Whole-tumour segmentation of all lesions was performed by a radiologist with 6 years of experience in head and neck imaging. To evaluate the interobserver reproducibility of the ADC parameters of conventional measurement and histogram analysis, 70 randomly selected lesions were analysed again by a radiologist with 8 years of experience in head and neck imaging. Intraclass correlation coefficients (ICCs) were calculated for each parameter, and the reproducibility was interpreted based on the following scale: (1) ICC <0.4, poor; (2) 0.4≤ ICC ≥0.59, fair; (3) 0.6< ICC ≥0.75, good; and (4) ICC ≥0.75, excellent.[12]

Statistical analysis

All statistical analyses were performed using R software (v. 3.5.2; www.r-project.org) (R Foundation for Statistical Computing, Vienna, Austria). Comparisons of clinical characteristics between two groups were evaluated using *t* tests, the Mann–Whitney *U* test or the χ^2 test, as appropriate. The Kolmogorov–Smirnov test was used to assess the normal distribution of continuous data. The ADC-associated parameters of two groups were compared using the Mann–Whitney *U* test. Stepwise logistic regression analysis was used to identify independent variables for predicting MT-IP. Based on the morphological features alone and with histogram parameters, respectively, two predictive models were built, using a primary cohort. Receiver operating characteristic (ROC) curves were used to assess the predictive performances of the significant features and the models, and areas under the ROC curve (AUCs) of the models were compared using the DeLong test. The nomogram for identifying MT-IP was plotted based on the optimal model. Calibration curves were plotted by bootstrapping with 1000 resamples for assessing the calibration of the nomogram, accompanied by the Hosmer–Lemeshow test. Decision curve analysis was used to calculate the net benefit from the use of two models at different threshold probabilities in the validation cohort. For all statistics, $p < 0.05$ was indicative of statistical significance.

Results

The primary cohort included 140 patients, 90 with IPs and 50 with MT-IPs. The validation cohort included 69 patients, 45 with IPs and 24 with MT-IPs. No significant difference was found in the percentage of MT-IPs ($p = 0.983$), sex ($p = 0.183$) or age ($p = 0.966$) between the primary and validation cohorts. All four morphological MRI features exhibited significant differences between two groups in both cohorts (all $p < 0.001$). A comparison of the clinical characteristics and morphological MRI features is given in Table 1.

In the reproducibility analysis, seven histogram parameters (the exception was $ADC_{Entropy}$) exhibited excellent interobserver agreement (Table 2). In comparisons of parameters between the two groups, ADC_{Mean}, ADC_{Median}, ADC_{10th}, ADC_{90th} and $ADC_{Entropy}$ were significantly smaller in patients with MT-IP in both cohorts (all $p < 0.05$). In addition, $ADC_{Skewness}$ and $ADC_{Uniformity}$ were significantly larger in patients with MT-IP in both cohorts (all $p < 0.05$). Representative cases are shown in Figure 1. Comparisons of ADC parameters between the two groups are given in Table 2 and Figure 2.

By combining morphological MRI features and ADC histogram parameters in the analysis, the maximum diameter ($p < 0.001$), loss of CCP ($p = 0.032$), ADC_{10th} ($p < 0.001$) and $ADC_{Skewness}$ ($p = 0.011$) were identified as independent variables. Of these significant variables, ADC_{10th} gave the best-predictive performance, with AUCs of 0.90 and 0.94 in the primary and validation cohorts, respectively. The maximum diameter, loss of CCP and $ADC_{Skewness}$ achieved AUCs of 0.80, 0.77 and 0.81, respectively, in the primary cohort and 0.79, 0.72 and 0.75, respectively, in the validation cohort.

The nomogram combining ADC histogram parameters and morphological features showed significantly better predictive performance than the model based on morphological features alone (AUCs, 0.96 *vs* 0.88, $p = 0.006$) and validation cohort (AUCs, 0.96 *vs* 0.88, $p = 0.015$) (Table 3 and Figure 3). The calibration curve showed good calibration in the primary cohort, with

Table 1 Clinical characteristics and morphological MRI features of patients

	Primary cohort (n = *140*)			*Validation cohort* (n = *69*)		
	IP (n = *90*)	*MT-IP* (n = *50*)	p	*IP* (n = *45*)	*MT-IP* (n = *24*)	p
Sex			0.906			0.789
Male	68 (75.8%)	39 (78.8%)		29 (63.8%)	17 (70.8%)	
Female	22 (24.2%)	11 (21.2%)		16 (36.2%)	7 (29.2%)	
Age (years)	56 ± 12	58 ± 12	0.289	56 ± 14	59 ± 12	0.334
Maximum diameter (mm)	47.7 ± 13.6	62.9 ± 13.7	<0.001	48.1 ± 14.7	67.4 ± 19.5	<0.001
Bony erosion			<0.001			<0.001
Yes	8 (8.9%)	25 (50.0%)		6 (13.3%)	13 (54.2%)	
No	82 (91.1%)	25 (50.0%)		39 (86.7%)	11 (45.8%)	
Orbit or intracranial invasion			<0.001			<0.001
Yes	5 (5.6%)	18 (36.0%)		2 (4.4%)	9 (37.5%)	
No	85 (94.4%)	32 (64.0%)		43 (95.6%)	15 (62.5%)	
Loss of convoluted cerebriform pattern			<0.001			<0.001
Yes	19 (21.1%)	38 (76.0%)		8 (17.8%)	19 (79.2%)	
No	71 (78.9%)	12 (24.0%)		37 (82.2%)	5 (20.8%)	

CCP, convoluted cerebriform pattern; IP, inverted papilloma; MT-IP, inverted papilloma with malignant transformation
Data are presented as *n* (%) or mean ± standard deviation.

Table 2 Comparison of ADC histogram parameters between two groups (with and without malignant transformation)

		Primary cohort			*Validation cohort*		
Parameter (10^{-3} mm²/s)	*ICC*	*IP*	*MT-IP*	p	*IP*	*MT-IP*	p
ADC_{Mean}	0.99	1.46 (1.30, 1.61)	1.17 (1.06, 1.34)	<0.001	1.45 (1.36, 1.53)	1.15 (1.04, 1.25)	<0.001
ADC_{Median}	0.99	1.44 (1.28, 1.59)	1.10 (0.96, 1.29)	<0.001	1.43 (1.30, 1.50)	1.10 (1.02, 1.22)	<0.001
ADC_{10th}	0.98	1.16 (1.04, 1.28)	0.83 (0.74, 0.91)	<0.001	1.15 (1.05, 1.23)	0.82 (0.69, 0.96)	<0.001
ADC_{90th}	0.96	1.81 (1.65, 1.98)	1.61 (1.37, 1.89)	<0.001	1.81 (1.70, 1.93)	1.53 (1.41, 1.67)	<0.001
$ADC_{Skewness}$	0.85	0.35 (0.02, 0.60)	0.86 (0.51, 1.16)	<0.001	0.32 (0.17, 0.59)	0.70 (0.48, 1.00)	<0.001
$ADC_{Kurtosis}$	0.89	4.14 (3.42, 4.85)	4.55 (3.84, 5.68)	0.029	3.89 (3.40, 5.63)	5.35 (4.03, 5.93)	0.059
$ADC_{Uniformity}$	0.75	0.038 (0.033, 0.043)	0.044 (0.039, 0.052)	<0.001	0.036 (0.032, 0.049)	0.049 (0.039, 0.058)	0.002
$ADC_{Entropy}$	0.63	4.99 (4.78, 5.17)	4.85 (4.66, 4.98)	0.001	5.03 (4.67, 5.17)	4.65 (4.49, 4.94)	0.006

ADC, apparent diffusion coefficient; ICC, intraclass correlation coefficient; IP, inverted papilloma; MT-IP, inverted papilloma with malignant transformation
Data are reported as median (interquartile range).

a non-significant Hosmer–Lemeshow test result (p = 0.238); this was verified by the validation cohort (p = 0.805) (Figure 4). The decision curve analysis showed that the nomogram provided a better net benefit to predict MT-IP, compared with the morphological model and with scenarios in which no prediction model would be used (*i.e.* treat-all or treat-none schemes) (Figure 5).

Discussion

It is challenging to discriminate sinonasal IP from MT-IP but of great importance. Our results indicate that a nomogram incorporating morphological features (maximum diameter and loss of CCP) and ADC histogram parameters (ADC_{10th} and $ADC_{Skewness}$) exhibited better predictive performance than a model using morphological features alone. Furthermore, the nomogram had good calibration in both cohorts and was confirmed as clinically useful.

Maps of ADC can quantitatively assess the Brownian motion of water molecules, closely indicating the tumour microenvironment with regard to water content and tumour cellularity.[13] In this study, all ADC values (mean, median and percentile values) were significantly smaller in patients with MT-IP than in patients with IP. In agreement with previous studies,[8,11] smaller ADC values are associated with more significant tumour cell proliferation, indicating the presence of more aggressive biological behaviour in MT-IP. Whole-tumour histogram analysis can provide comprehensive information on the tissue characteristics of the entire tumour and has been used to evaluate sinonasal tumours.[11,14,15] In our study, ADC_{10th} demonstrated better performance than other histogram parameters. Previous studies have indicated that lower percentiles of an ADC histogram had greater advantages in the classification and grading of tumours than higher percentiles.[11,16,17] A recent study reported that ADC_{10th} could serve as a promising biomarker for predicting occult lymph node metastasis in the early stage of head and neck cancer.[12] Given our similar results, it is possible that the tumour biological behaviour is more truly reflected by the diffusion characteristics of densely packed solid tumours. Therefore, it could be more accurately evaluated by low percentiles of the ADC histogram, which is less affected by the components of microcystic degeneration, necrosis and oedema. In our study, the $ADC_{Skewness}$ of MT-IP was higher than that of IP in both cohorts, showing that it could be identified as an independent predictor. As an index measuring the asymmetrical distribution of the ADC histogram, a higher positive skewness indicates that the voxel values cluster towards the

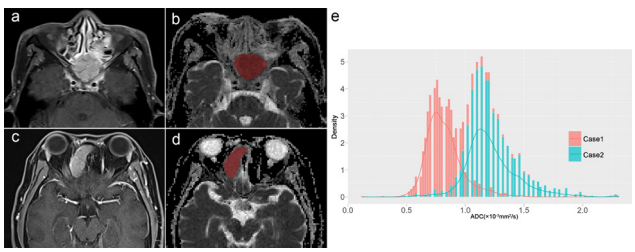

Figure 1 A 67-year-old male (Case 1) and (c, d) a 40-year-old female (Case 2) were pathologically confirmed as having MT-IP and IP, respectively; (b, d) the whole-tumour ROIs of ADC were delineated by referral to (a, c) contrast-enhanced T_1 weighted imaging; (e) two ADC histograms were acquired based on the ROIs, and a lower ADC_{10th} (0.68×10^{-3} mm²/s *vs* 1.01×10^{-3} mm²/s) and higher $ADC_{Skewness}$ (0.92 *vs* 0.29) were shown in Case 1, compared with Case 2. ADC, apparent diffusion coefficient; IP, inverted papilloma; MT, malignant transformation; MT-IP, inverted papilloma with malignant transformation; ROIs, regions of interest.

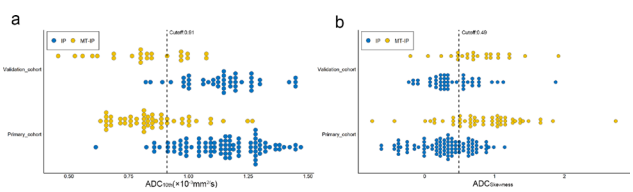

Figure 2 Scatter plots of ADC_{10th} and $ADC_{Skewness}$: dotted lines demonstrate the best cutoff values for predicting MT-IP. ADC, apparent diffusion coefficient; MT-IP, inverted papilloma with malignant transformation.

Table 3 Predictive performance of significant variables and models

		Primary cohort			*Validation cohort*		
Variable or model	*Cut-off*	*AUC (95% CI)*	*Sensitivity*	*Specificity*	*AUC (95% CI)*	*Sensitivity*	*Specificity*
Maximum diameter (mm)	51	0.80 (0.72, 0.86)	0.86	0.71	0.79 (0.68, 0.88)	0.96	0.49
Loss of convoluted cerebriform pattern		0.77 (0.70, 0.85)	0.76	0.79	0.72 (0.61, 0.84)	0.63	0.82
ADC_{10th} ($\times 10^{-3}$ mm²/s)	0.91	0.90 (0.84, 0.95)	0.76	0.91	0.94 (0.86, 0.98)	0.92	0.82
$ADC_{Skewness}$	0.49	0.81 (0.73, 0.87)	0.8	0.7	0.75 (0.63, 0.85)	0.88	0.6
Morphological model		0.88 (0.81, 0.94)	0.8	0.87	0.88 (0.81, 0.96)	0.75	0.89
Nomogram		0.96 (0.93, 0.99)	0.92	0.92	0.96 (0.91, 0.99)	0.96	0.87

ADC, apparent diffusion coefficient; AUC, area under receiver operating characteristic curve; CI, confidence interval
Data in parentheses indicate 95% CIs. Morphological model was constructed by maximum diameter and loss of convoluted cerebriform pattern. Nomogram was constructed by maximum diameter, loss of convoluted cerebriform pattern, ADC_{10th} and $ADC_{Skewness}$.

lower end. Previous studies have indicated significantly larger $ADC_{Skewness}$ results in high-grade compared with low-grade renal cell carcinomas[18] and head and neck cancers.[19] Our observation of higher ADC skewness in MT-IPs reflected a predominance of smaller ADCs associated with neoplasia-related cellularity.

As morphological features, maximum diameter and loss of CCP showed significant differences between IPs and MT-IPs in both cohorts. However, two ADC histogram parameters were also selected as independent predictors. In addition, on comparing the predictive performance of the two models, the nomogram incorporating morphological features and ADC histogram parameters exhibited better performance than the model using morphological features alone in both the primary cohort (AUCs, 0.96 *vs* 0.88) and validation cohort (AUCs, 0.96 *vs* 0.88). These results further suggest that ADC maps may provide powerful supplementary information in the diagnosis of MT-IP. Recently, dynamic contrast-enhanced MRI was reported to be useful to predict sinonasal MT-IP, with the optimal AUC of 0.83 being weaker than those of our two models.[20] Moreover, compared with dynamic contrast-enhanced MRI, DWI is a better fit for routine use because of its shorter examination time. Furthermore, the nomogram also showed good calibration in the validation cohort. These results suggest that the nomogram is a reliable and reproducible tool for identifying MT-IP. In addition, decision curve analysis was applied in this study. The decision curve showed that the application of nomogram to predict MT-IPs added more benefit than treating all or none of the patients, or than using a morphological model.

This study has some limitations: First, our results were from a single-centre study and further prospective multicentre studies are required to obtain high-level evidence for clinical application. Second, sample selection bias, such as small tumour size and low image quality, may

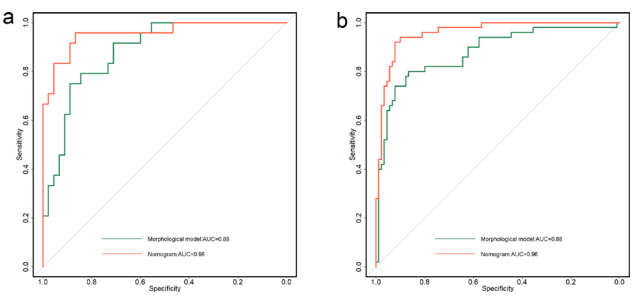

Figure 3 Comparison of receiver operating characteristic curves of two models in (a) primary and (b) validation cohorts, respectively. ADC, apparent diffusion coefficient; AUC, area under curve; CCP, convoluted cerebriform pattern; MT-IP, inverted papilloma with malignant transformation.

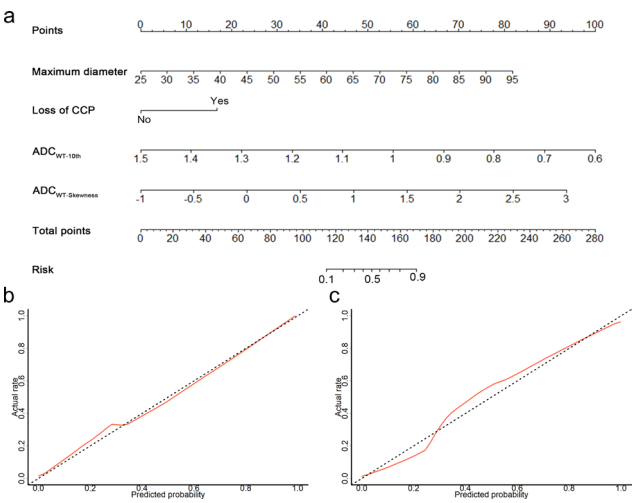

Figure 4 (a) By combining maximum diameter, loss of CCP, ADC_{10th} and $ADC_{Skewness}$, a nomogram was developed in the primary cohort, with good calibration curves in both (b) the primary cohort and (c) the validation cohort. ADC, apparent diffusion coefficient; CCP, convoluted cerebriform pattern.

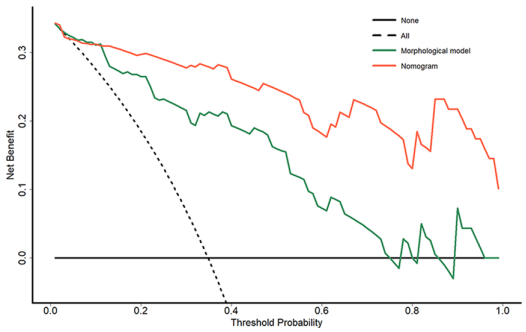

Figure 5 Decision curve analysis for each model in the validation cohort: the *y*-axis measures the net benefit, which is calculated by summing the benefits (true-positive findings) and subtracting the harms (false-positive findings) and weighting the latter by a factor related to the relative harm of undetected MT-IP compared with the harm of unnecessary treatment; the decision curve showed that the application of nomogram to predict MT-IPs added more benefit than treating all or none of the patients or using the morphological model. MT-IP, inverted papilloma with malignant transformation.

exist in this study because of the exclusion criteria used. This also partly explains the higher rate of MT reported in this study, compared with previous studies.[1] Third, the ROIs were placed manually, depending on the individual experience of the radiologist. Finally, only conventional DWI with a monoexponential model was used in our study; this could have been influenced by tissue microperfusion. The value of advanced diffusion models in predicting MT-IP, such as intravoxel incoherent motion MRI and diffusion kurtosis imaging, should be further investigated in future studies.

Conclusion

Incorporating morphological MRI features and ADC histogram parameters in an easy-to-use nomogram facilitates preoperative estimation of the risk of MT-IP. The nomogram could serve as a promising non-invasive tool and might guide future clinical practice.

Acknowledgment

This work was supported by the National Scientific Foundation of China (grant number 82101992).

Contributors

Jiliang Ren: Guarantor of integrity of the entire study; Study concepts and design; Manuscript revising; Meng Qi: Literature research; Data acquisition ; Data analysis; Manuscript Drafting; Zhipeng Xia: Statistical analysis; Data acquisition; Fang Zhang: Literature research; Data analysis; Yan Sha: Study concepts and design.

Competing interests

The authors declare that they have no conflict of interest.

REFERENCES

1. Mirza S, Bradley PJ, Acharya A, Stacey M, Jones NS. Sinonasal inverted papillomas: recurrence, and synchronous and metachronous malignancy. *J Laryngol Otol* 2007; **121**: 857–64. https://doi.org/10.1017/S002221510700624X
2. Contrera KJ, Woody NM, Rahman M, Sindwani R, Burkey BB. Clinical management of emerging sinonasal malignancies. *Head Neck* 2020; **42**: 2202–12. https://doi.org/10.1002/hed.26150
3. Lee JJ, Peterson AM, Embry TW, Wamkpah NS, Kallogjeri D, Doering MM, et al. Survival outcomes of de novo vs inverted papilloma-associated sinonasal squamous cell carcinoma: a systematic review and meta-analysis. *JAMA Otolaryngol Head Neck Surg* 2021; **147**: 350–59. https://doi.org/10.1001/jamaoto.2020.5261
4. Han MW, Lee BJ, Jang YJ, Chung YS. Clinical value of office-based endoscopic incisional biopsy in diagnosis of nasal cavity masses. *Otolaryngol Head Neck Surg* 2010; **143**: 341–47. https://doi.org/10.1016/j.otohns.2010.05.019
5. Gencturk M, Ozturk K, Caicedo-Granados E, Li F, Cayci Z. Application of diffusion-weighted MR imaging with ADC measurement for distinguishing between the histopathological types of sinonasal neoplasms. *Clin Imaging* 2019; **55**: 76–82. https://doi.org/10.1016/j.clinimag.2019.02.004
6. Das A, Bhalla AS, Sharma R, Kumar A, Thakar A, Vishnubhatla SM, et al. Can diffusion weighted imaging aid in differentiating benign from malignant sinonasal masses?: a useful adjunct. *Pol J Radiol* 2017; **82**: 345–55. https://doi.org/10.12659/PJR.900633
7. Daga R, Kumar J, Pradhan G, Meher R, Malhotra V, Khurana N. Differentiation of benign from malignant sinonasal masses using diffusion weighted imaging and dynamic contrast enhanced magnetic resonance imaging. *Am J Rhinol Allergy* 2022; **36**: 207–15. https://doi.org/10.1177/19458924211040602
8. Yan CH, Tong CCL, Penta M, Patel VS, Palmer JN, Adappa ND, et al. Imaging predictors for malignant transformation of inverted papilloma. *Laryngoscope* 2019; **129**: 777–82. https://doi.org/10.1002/lary.27582
9. Yu HX, Liu G. Malignant transformation of sinonasal inverted papilloma: a retrospective analysis of 32 cases. *Oncol Lett* 2014; **8**: 2637–41. https://doi.org/10.3892/ol.2014.2539
10. He W, Xiao X, Li X, Guo Y, Guo L, Liu X, et al. Whole-tumor histogram analysis of apparent diffusion coefficient in differentiating intracranial solitary fibrous tumor/hemangiopericytoma from angiomatous meningioma. *Eur J Radiol* 2019; **112**: 186–91. https://doi.org/10.1016/j.ejrad.2019.01.023
11. Suh CH, Lee JH, Chung MS, Xu XQ, Sung YS, Chung SR, et al. Mri predictors of malignant transformation in patients with inverted papilloma: a decision tree analysis using conventional imaging features and histogram analysis of apparent diffusion coefficients. *Korean J Radiol* 2021; **22**: 751–58. https://doi.org/10.3348/kjr.2020.0576
12. Ren J, Yuan Y, Tao X. Histogram analysis of diffusion-weighted imaging and dynamic contrast-enhanced MRI for predicting occult lymph node metastasis in early-stage oral tongue squamous cell carcinoma. *Eur Radiol* 2022; **32**: 2739–47. https://doi.org/10.1007/s00330-021-08310-0

13. Koh DM, Collins DJ. Diffusion-Weighted MRI in the body: applications and challenges in oncology. *AJR Am J Roentgenol* 2007; **188**: 1622–35. https://doi.org/10.2214/AJR.06.1403
14. Xiao Z, Tang Z, Zhang J, Yang G, Zeng W, Luo J, et al. Whole-tumor histogram analysis of monoexponential and advanced diffusion-weighted imaging for sinonasal malignant tumors: correlations with histopathologic features. *J Magn Reson Imaging* 2020; **51**: 273–85. https://doi.org/10.1002/jmri.26857
15. Fujima N, Kameda H, Tsukahara A, Yoshida D, Sakashita T, Homma A, et al. Diagnostic value of tumor blood flow and its histogram analysis obtained with pcasl to differentiate sinonasal malignant lymphoma from squamous cell carcinoma. *Eur J Radiol* 2015; **84**: 2187–93. https://doi.org/10.1016/j.ejrad.2015.07.026
16. Zhang W, Zhou Y, Xu X-Q, Kong L-Y, Xu H, Yu T-F, et al. A whole-tumor histogram analysis of apparent diffusion coefficient maps for differentiating thymic carcinoma from lymphoma. *Korean J Radiol* 2018; **19**: 358–65. https://doi.org/10.3348/kjr.2018.19.2.358
17. Ren J, Yuan Y, Wu Y, Tao X. Differentiation of orbital lymphoma and idiopathic orbital inflammatory pseudotumor: combined diagnostic value of conventional MRI and histogram analysis of ADC maps. *BMC Med Imaging* 2018; **18**(1): 6. https://doi.org/10.1186/s12880-018-0246-8
18. Kierans AS, Rusinek H, Lee A, Shaikh MB, Triolo M, Huang WC, et al. Textural differences in apparent diffusion coefficient between low- and high-stage clear cell renal cell carcinoma. *AJR Am J Roentgenol* 2014; **203**: W637–44. https://doi.org/10.2214/AJR.14.12570
19. Ren J, Qi M, Yuan Y, Tao X. Radiomics of apparent diffusion coefficient maps to predict histologic grade in squamous cell carcinoma of the oral tongue and floor of mouth: a preliminary study. *Acta Radiol* 2021; **62**: 453–61. https://doi.org/10.1177/0284185120931683
20. Li Z, Xian M, Guo J, Wang CS, Zhang L, Xian J. Dynamic contrast-enhanced MRI can quantitatively identify malignant transformation of sinonasal inverted papilloma. *Br J Radiol* 2022; **95**(1134): 20211374. https://doi.org/10.1259/bjr.20211374